XFAIMS– eXternal Field Ab Initio Multiple Spawning for electron-nuclear dynamics triggered by short laser pulses

Benoit Mignolet[1], Basile F. E. Curchod[2,a)] and Todd J. Martínez[3,4,b)]
[1] *Department of Chemistry, University of Liège, 4000 Liège, Belgium*
[2] *Centre for Computational Chemistry, School of Chemistry, University of Bristol, UK.*
[3] *Department of Chemistry and the PULSE Institute, Stanford University, Stanford, CA 94305, USA.*
[4] *SLAC National Accelerator Laboratory, Menlo Park, CA 94025, USA.*
[a)] *Email: basile.curchod@gmail.com,* [b)] *Email: toddjmartinez@gmail.com*

Attoscience is an emerging field where attosecond pulses or few cycle IR pulses are used to pump and probe the correlated electron-nuclear motion of molecules. We present the trajectory-guided eXternal Field Ab Initio Multiple Spawning (XFAIMS) method that models such experiments "on-the-fly," from laser pulse excitation to fragmentation or nonadiabatic relaxation to the ground electronic state. For the photoexcitation of the LiH molecule, we show that XFAIMS gives results in close agreement with numerically exact quantum dynamics simulations, both for atto- and femtosecond laser pulses. We then show the ability of XFAIMS to model the dynamics in polyatomic molecules by studying the effect of nuclear motion on the photoexcitation of sulfine (H_2SCO).

Over the last decade, the development of attosecond and few cycle femtosecond IR pulses paved the way for probing electronic motion in atoms and molecules.[1-3] Pump-probe schemes combining an IR pulse with an isolated attosecond pulse,[4-5] or attosecond pulse trains,[6-7] have been used to induce and probe dynamics in small molecules. Despite the attosecond moniker, the time-scale of such experiments usually spans several tens of femtoseconds or more because of the longer IR pulse or train of attosecond pulses used to either excite or probe the molecule. This leads to a complex interplay between electronic and nuclear dynamics that complicates analysis even for diatomic molecules.[8] Furthermore, the electronic dynamics is usually probed indirectly through fragmentation patterns. Unraveling the complex laser-induced electron-nuclear dynamics requires methods that model the entire experiment from laser excitation through to relaxation or fragmentation.

Several methods are able to describe the correlated electronic-nuclear dynamics induced by a laser pulse, including numerically-exact grid-based methods.[9] However, most of these are limited to diatomic[10-12] or small polyatomic[13] molecules. For larger molecules, real-time time-dependent density functional theory (TDDFT)[14-17] and trajectory surface hopping[18-22] have been used to model field-induced dynamics. In RT-TDDFT, electron-nuclear dynamics is modeled using a mean-field Ehrenfest approach. Unfortunately, RT-TDDFT cannot accurately describe fragmentation or nonadiabatic dynamics that can occur after the pulse. Surface hopping[19,22-23] using the "fewest-switches" algorithm[24] (TSH) requires a double averaging of the trajectories: over the initial conditions and over the hopping events. Therefore a large number of trajectories are required to obtain a converged branching ratio,[25-27] or pulse-induced population transfer, especially if this excited population is small. Furthermore, TSH neglects certain phase interferences that might be dynamically important.

In this Communication, we present eXternal Field Ab Initio Multiple Spawning (XFAIMS), based on the AIMS method.[28-30] XFAIMS models a complete photochemical experiment, from the excitation of a molecule by one or several laser pulses to subsequent nonradiative relaxation or fragmentation. We compare XFAIMS to numerically-exact grid-based quantum dynamics for the photoexcitation of LiH from its ground electronic state S_0 to its first excited state S_1. The high anharmonicity of the S_1 potential energy curve (Fig. 1) makes the description of correlated electron-nuclear dynamics challenging, especially when the S_1 nuclear wavepacket leaves the Franck-Condon region. We further investigate the electron-nuclear dynamics triggered by either a subfemtosecond UV pulse or a 10fs IR pulse. Finally, XFAIMS is applied to full-dimensional simulation of photoexcitation in a polyatomic - sulfine (H_2CSO).[31-32]

Theory: As in AIMS,[28-29,33] the time-dependent nuclear wavefunctions in XFAIMS are expanded in a basis of state-specific Gaussian nuclear basis functions with frozen width (α), called trajectory basis functions (TBFs):[28,33]

$$\Psi(\mathbf{r},\mathbf{R},t)=\sum_I \sum_{j=1}^{N_I(t)} C_I^j(t)\chi_I^j\left(\mathbf{R};\bar{\mathbf{R}}_I^j(t),\bar{\mathbf{P}}_I^j(t),\bar{\gamma}_I^j(t),\alpha\right)\phi_I(\mathbf{r};\mathbf{R}) \quad (1)$$

The summation indices I and j run over electronic states $\phi_I(\mathbf{r};\mathbf{R})$ and TBFs χ_I^j, respectively. The time-dependent average position $\bar{\mathbf{R}}_I^j(t)$ and momentum $\bar{\mathbf{P}}_I^j(t)$ are propagated classically on adiabatic potential energy surfaces, while the phase factor $\bar{\gamma}_I^j(t)$ is propagated semi-classically. Other propagation schemes could also be considered. For example, the TBFs could be propagated using Ehrenfest equations of motion during the pulse as in the *ab initio* multiple cloning (AIMC) method.[34]

When electronic states become strongly coupled, either due to a conical intersection or, central in this work, due to the electric field of the pulse, new TBFs are spawned on the relevant electronic states. Therefore the number of TBFs on electronic state I, N_I(t), varies with time during the dynamics. Inserting the wavefunction of Eq. (1) into the

molecular time-dependent Schrödinger equation (TDSE) leads to the following set of coupled equations for the evolution of the TBF amplitudes $C_I^j(t)$:

$$\frac{d\mathbf{C}_I(t)}{dt} = -i\left(\mathbf{S}_{II}^{-1}\right)\left\{\left[\mathbf{H}_{II}^{Intra} - i\dot{\mathbf{S}}_{II}\right]\mathbf{C}_I(t) + \sum_{J\neq I}\mathbf{H}_{IJ}^{Inter}\mathbf{C}_J(t)\right\} \quad (2)$$

The vector $\boldsymbol{C}_I$(t) contains the amplitudes of all TBFs evolving on the Ith electronic state. The inverse of the overlap matrix, $\mathbf{S}^{-1}$, and its time-derivative, $\dot{\mathbf{S}}$, arise from the nonorthogonality of the Gaussian functions, as described (along with further details of AIMS) in previous work.[28,33]

The Hamiltonian matrix coupling the different TBFs can be separated into interstate (TBFs on different electronic states) and intrastate (TBFs on the same electronic state) parts. The intrastate coupling elements are composed of the (field-free) electronic energy, the nuclear kinetic energy, and the field-induced coupling that involves the scalar product of the electric field with the electronic and nuclear dipole moment (computed as described previously[34]):

$$\left(\mathbf{H}_{II}^{Intra}\right)_{kl} = \left\langle\chi_I^k\middle|E_I^{el}\middle|\chi_I^l\right\rangle_{\mathbf{R}} - \left\langle\chi_I^k\middle|\sum_{\rho=1}^{3N}\frac{\partial^2}{2m_\rho\partial R_\rho^2}\middle|\chi_I^l\right\rangle_{\mathbf{R}} - \vec{\mathbf{E}}(t)\cdot\left\langle\chi_I^k\middle|\vec{\mu}_{II}^{elec} + \vec{\mu}^{nuc}\middle|\chi_I^l\right\rangle_{\mathbf{R}} \quad (3)$$

where the index ρ runs over the 3N coordinates of the molecule with N atoms. The time-dependent electric field of the pulse, $\vec{\mathbf{E}}(t)$, is defined from the derivative of the vector potential:

$$\vec{\mathbf{E}}(t) = -\frac{1}{c}\frac{d\vec{\mathbf{A}}(t)}{dt} \quad (3)$$

In the simulations below, we used a Gaussian-shaped pulse:

$$\vec{\mathbf{A}}(t) = \vec{\varepsilon}\left(cf_0/\omega\right)\exp\left[\frac{-(t-t_0)^2}{2\sigma^2}\right]\sin\left(\omega t + CEP\right) \quad (3)$$

where $\vec{\varepsilon}$ is the polarization vector, c the speed of light, t_0 the time at which the pulse is centered, f_0 is the field strength, $\boldsymbol{\omega}$ is the carrier frequency and the pulse length is given by σ. The full width at half maximum (FWHM) of the pulse is 2.35σ. The carrier envelope phase (CEP) is the phase difference between the pulse envelope and the oscillation of the electric field. For few cycle pulses, the CEP controls the waveform (sub-femtosecond evolution) of the pulse and can affect the dynamics.[35-36]

The interstate coupling includes the nonadiabatic coupling matrix elements ($\mathbf{d}_{IJ}$) and the coupling between electronic states due to the electric field (intra- and interstate second-order nonadiabatic couplings are neglected):

$$\left(\mathbf{H}_{IJ}^{Inter}\right)_{kl} = -\left\langle\chi_I^k\middle|\sum_{\rho}^{3N}d_{IJ}^{\rho}\frac{1}{m_\rho}\frac{\partial}{\partial R_\rho}\middle|\chi_J^l\right\rangle_{\mathbf{R}} - \vec{\mathbf{E}}(t)\cdot\left\langle\chi_I^k\middle|\vec{\mu}_{IJ}^{elec}\middle|\chi_J^l\right\rangle_{\mathbf{R}} \quad (3)$$

The transfer of amplitude between electronic states during the pulse depends on the transition dipole moment modulated by $\vec{\mathbf{E}}(t)$ and the nuclear overlap between the TBFs. Eq. (2) is equivalent to the exact TDSE in the limit of a large number of TBFs and is at the heart of the Full Multiple Spawning (FMS) method. In practice, two central approximations are required for molecular applications. First, a zeroth-order saddle-point approximation (SPA) is used to evaluate the Hamiltonian matrix elements. Second, the initial (parent) TBFs are considered uncoupled and will be run independently. It is however important to note that all the children TBFs produced by a given parent TBF will be coupled, i.e., only the TBFs produced by different parents are uncoupled. This independent first generation (IFG)

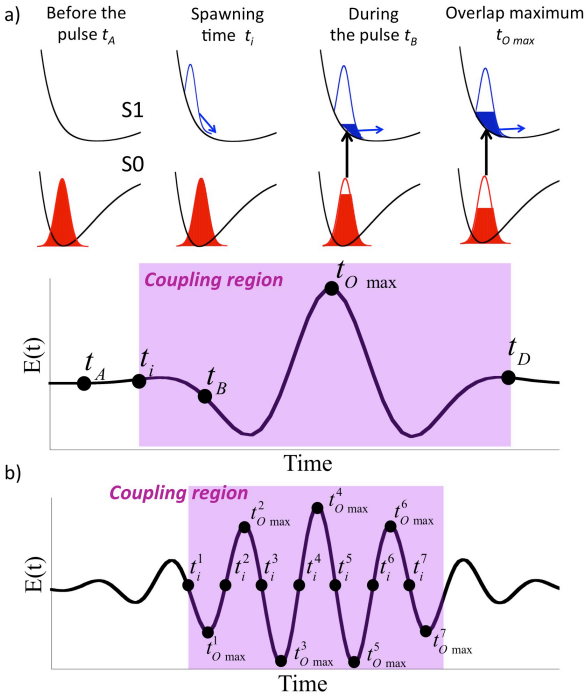

Fig. 1: Schematic representation of the spawning method during the pulse. The S_0 and S_1 potential energy surfaces of LiH are computed at the SA2-CASSCF(4/6)/6-31G level. In panel a), only one TBF is spawned, at the time t_{Omax}, when the pulse is maximum. In panel b) a new TBF is spawned every time the electric field reaches a maximum, twice per optical period. The area in purple represents the region where new basis functions can be spawned if required.

approximation is based on the observation that for multidimensional systems, the initial nuclear wavepacket is expected to rapidly spread over the molecular configuration space, i.e., parent TBFs will rapidly separate. Combining the SPA and IFG approximations with on-the-fly electronic structure calculations in FMS leads to the AIMS method.[28]

A key element of the XFAIMS method is the spawning algorithm, which was adapted from the original AIMS method to account for couplings resulting from the interaction of a molecule with laser pulses. Two limiting cases can be identified based on the overall length of the laser pulse and on the fact that parent and child TBFs should overlap during the interaction. Nuclear motion during a short pulse is not expected to be significant, hence spawning of a single TBF on S_1 can be sufficient in this case (see Fig. 1a and 1b). The spawning process starts when the field envelope is larger than a predefined threshold (time t_i in Fig. 1a). The parent TBF is independently propagated forward in time according to Hamilton's equations of motion until the electric field drops below the threshold (time t_D). At the

maximum of the Gaussian field envelope (time t_{0max}), a TBF is spawned on S_1 and back-propagated until the entry time t_i. During the spawn, the kinetic energy of the child TBF is not adjusted (as would often be done in conventional AIMS describing field-free nonadiabatic effects). Finally, the overall wavepacket – constituted by the TBFs in S_0 and S_1 – is propagated forward in time and transfer of amplitude due to the electric field of the pulse can occur. In the second limit of a longer pulse (Fig. 1c), several TBFs must be spawned during the pulse to ensure that at least one child TBF overlaps with the parent TBF throughout the field-induced interaction period. In this second type of spawning algorithm, a new TBF is spawned each time the field reaches a maximum or a minimum, i.e., twice per cycle. Spawning is prevented if the overlap between TBFs on the two electronic states is too large or if the population of the parent TBF is too small.

In the context of the photoexcitation by a laser pulse, we analyze the time-dependent population and dipole moment. The population of an electronic state I is given by

$$n_I(t) = \sum_{j}^{N_I(t)} \sum_{j'}^{N_I(t)} C_I^{j*}(t) C_I^{j'}(t) S_{II}^{jj'} \quad (4)$$

and the time-dependent dipole moment by

$$\vec{\mu}(t) = \sum_{I,I'}^{N} \sum_{j,j'}^{N_I(t)N_{I'}(t)} C_I^{j*}(t) C_{I'}^{j'}(t) \left[\vec{\mu}_{II'}^{elec}\left(\mathbf{R}_{jj'}^{centroid}\right) S_{II'}^{jj'} + \vec{\mu}^{nuc}\left(\mathbf{R}_{jj'}^{centroid}\right) \delta_{II'} \right] \quad (4)$$

where N is the number of electronic states and the SPA has been invoked. The time-dependent dipole moment reflects the density of the coherent superposition of states. Due to interferences between electronic states, the dipole continues oscillating after the pulse is over[12,37-40] with an amplitude that is modulated by the overlap between TBFs (Fig. 2b).

Test Application: We first compare the XFAIMS method to grid-based numerically exact quantum dynamics simulations for the photoexcitation of the heteronuclear diatomic LiH (Fig. 1) by a short UV resonant pulse or an 8.5fs IR pulse. For the grid simulations, potential energy surfaces are pre-computed at the SA2-CASSCF(4/6)/6-31G level for S_0 and S_1. In XFAIMS, the electronic structure is computed on-the-fly with MOLPRO[33,41] at the same level of theory. The S_1 state has an anharmonic potential with an equilibrium LiH distance of 2.44 Å compared to 1.66 Å on S_0. We include only two electronic states in this example, but more states should be included if strong pulses are used and ionization needs to be described.[42-43] The simulations below are carried out for aligned molecules.

We compared the dynamics of LiH excited by a 0.85fs one-cycle UV resonant attopulse predicted by different methods. For the grid simulation, we started the dynamics on S_0 from the ground vibrational eigenstate of S_0 while for XFAIMS we started from a swarm of 100 Wigner-sampled initial conditions, using the IFG approximation. We also ran XFAIMS dynamics starting from a set of 5 initially-coupled TBFs with LiH distance ranging from 1.60Å to 1.72Å and no initial momentum. Finally we also ran XFAIMS at a frozen nuclear geometry[44-45] starting from the equilibrium geometry of LiH. We observed in all cases nearly identical population transfer during the pulse (Fig. 2a), and backtransfer from S_1 to S_0 is also well described. This was expected since the pulse is short (0.85fs) and there is no significant nuclear motion during the pulse. However the nuclear motion plays a major role on the dipole moment after the end of the pulse (Fig. 2b). When the nuclei are frozen, the dipole moment incorrectly oscillates with constant amplitude due to interferences between the two electronic states of the coherent superposition built by the pulse. The numerically-exact grid simulation including nuclear motion shows that the amplitude of the time-dependent dipole moment should decrease with time as the wavepacket on S_1 leaves the Franck-Condon (FC) region.[12] XFAIMS with moving nuclei and the IFG approximation yields a time-dependent dipole moment that agrees with the grid simulation for early and late times. At intermediate

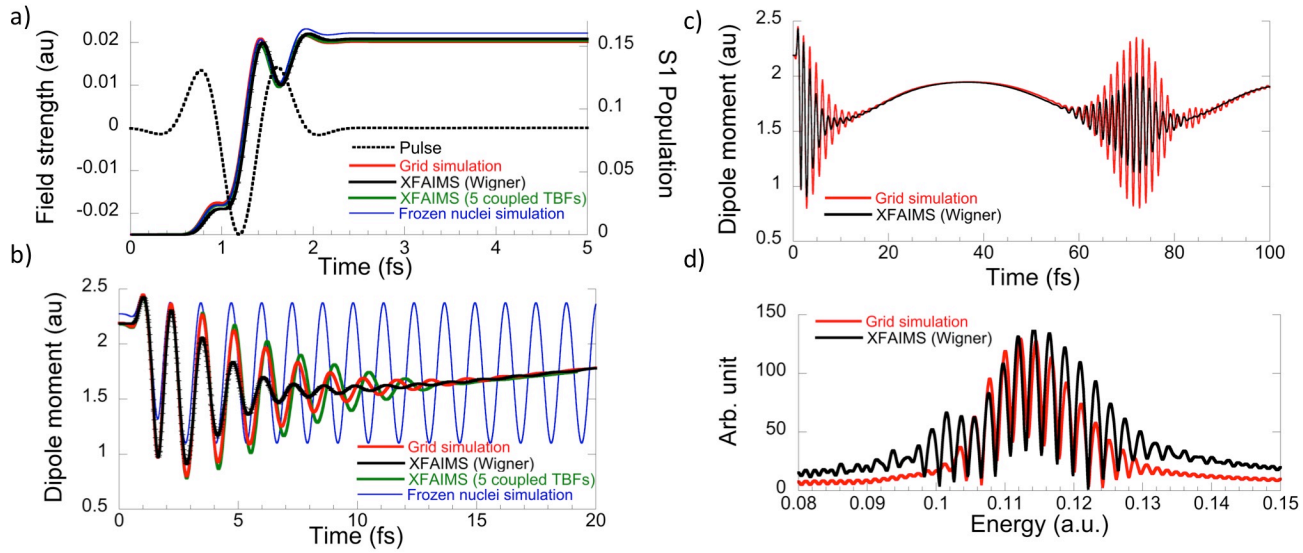

Fig. 2 a) S_1 population induced by a resonant UV pulse polarized along the molecular axis (f_0=0.025a.u., FWHM=0.84fs, ω=0.127a.u., CEP=π) computed at frozen nuclei geometry, on a grid, and with XFAIMS, the latter for a set of 100 uncoupled initial conditions sampled from a Wigner distribution and for a set of 5 coupled TBFs. Standard error is given for the Wigner-sampled XFAIMS calculations. b-c) Dipole moment along the molecular axis for the pulse of panel a) in a time-window of 20 and 100fs. d) Fourier transform of the dipole moment in panel c).

times (5-10fs), the amplitude of dipole moment oscillations is underestimated. A more accurate XFAIMS description is achieved by starting from five initially-coupled TBFs on S_0. This simulation both releases the IFG approximation and better describes the initial nuclear wavefunction, leading to quantitative agreement with the grid simulation.

The S_1 state is bound, so the wavepacket returns to the FC region after reaching the outer turning point, leading to interferences with the S_0 wavepacket.[12,39,46] This is reflected in the strong oscillations of the dipole moment between 70 and 80fs (Fig. 2c). XFAIMS somewhat underestimates the amplitude of these oscillations, potentially due to the IFG approximation, but the oscillations remain in phase with exact results even after 80fs. The Fourier transform of the dipole moment (Fig. 2d) exhibits a broad peak centered at the $S_0 \rightarrow S_1$ excitation energy, superimposed on a vibrational progression corresponding to excitation from S_0 to vibrationally excited states of S_1, as reported previously.[12,39]

We also assessed XFAIMS for a longer and more realistic pulse where nuclear motion is significant during the pulse (Fig. 3). We choose a weak (3×10^{12}W/cm^2) 8.5fs 800nm IR pulse that populates S_1 through 2 photon transitions. As for the short pulse, XFAIMS simulations start from 100 uncoupled Wigner-sampled initial conditions. The population transfer and time-dependence of the dipole moment are again in good agreement with the grid simulation (Fig. 3). As in the case of the short pulse, the XFAIMS-computed time-dependent dipole moment is somewhat underestimated at intermediate times (15-20 fs). However, the XFAIMS and exact time-dependent dipole moments are overall in excellent agreement.

As a last example, we use XFAIMS to model polyatomic electron-nuclear dynamics, which is the raison d'etre of this method. We investigated the effect of nuclear motion on population transfer of H_2CSO during photoexcitation to S_1 by short (0.85fs) and longer (2.54fs) resonant perpendicularly-polarized UV pulses (Fig. 4). The S_0 and S_1 electronic states are computed on the fly with SA2-CASSCF(4/3)/6-31G(d). The short pulse (Fig 4.a) leads to similar population transfer when the nuclei are frozen or allowed to move. For the longer pulse (Fig. 4b), population transfer is significantly overestimated when the nuclei are frozen.

Conclusions: XFAIMS efficiently and accurately describes coupled electron-nuclear dynamics from laser excitation through fragmentation/relaxation. Good agreement with numerically-exact quantum dynamics was achieved for the excitation of LiH molecule by resonant and non-resonant short and long pulses. We demonstrated the applicability of the method to a polyatomic molecule. XFAIMS paves the way towards complete *in silico* photochemical experiments of large molecules, especially given the emergence of GPU-accelerated electronic structure calculations.[47]

Acknowledgments: This work was supported by the AMOS program within the Chemical Sciences, Geosciences, and Biosciences Division of the Office of Basic Energy Sciences, Office of Science, US Department of Energy. The

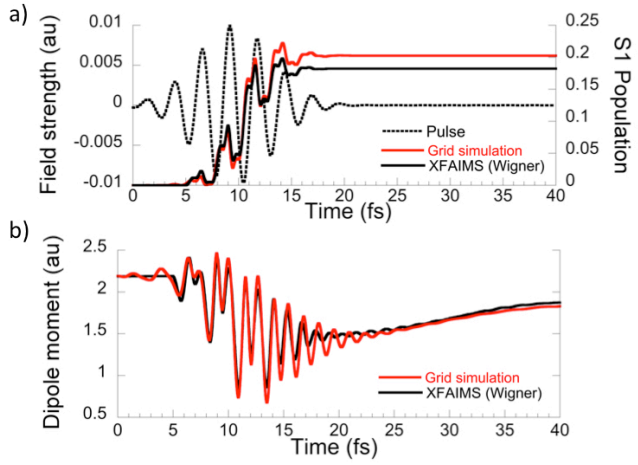

Fig. 3: a) S_1 population induced by a 8.5fs IR pulse polarized along the molecular axis (f_0=0.01a.u., FWHM=8.46fs, ω=0.0576a.u., CEP=π) computed on a grid and with XFAIMS. b) Dipole moment along the molecular axis for the pulse of panel a.

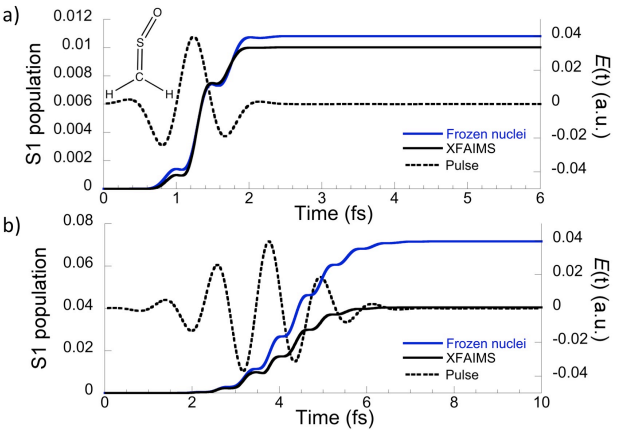

Fig. 4: a) S_1 population induced by a 0.85fs resonant UV pulse polarized perpendicularly to the molecular axis (f_0=0.04a.u., FWHM=0.85fs, ω=0.12a.u.). The sulfine molecule is shown in the inset. b) Same as a) for a 2.54fs pulse (f_0=0.04a.u., FWHM=2.54fs, ω=0.12 a.u.).

authors would like to acknowledge Francoise Remacle for fruitful discussions. B.M. gratefully acknowledges support from the Fonds National de la Recherche Scientifique (Belgium). B.F.E.C. is supported by the Marie Curie Research Grants Scheme, grant 701355 (NAMDIA).

References

1. M.F. Kling and M.J.J. Vrakking, *Ann. Rev. Phys. Chem.* **59**, 463 (2008).
2. F. Krausz and M. Ivanov, *Rev. Mod. Phys.* **81**, 163 (2009).
3. F. Lépine, G. Sansone and M.J.J. Vrakking, *Chem. Phys. Lett.* **578**, 1 (2013).
4. G. Sansone, F. Kelkensberg, J.F. Perez-Torres, F. Morales, M.F. Kling, W. Siu, O. Ghafur, P. Johnsson, M. Swoboda, E. Benedetti, F. Ferrari, F. Lepine, J.L. Sanz-Vicario, S. Zherebtsov, I. Znakovskaya, A. L/'Huillier, M.Y. Ivanov, M. Nisoli, F. Martin and M.J.J. Vrakking, *Nature* **465**, 763 (2010).

5. F. Calegari, D. Ayuso, A. Trabattoni, L. Belshaw, S. De Camillis, S. Anumula, F. Frassetto, L. Poletto, A. Palacios, P. Decleva, J.B. Greenwood, F. Martín and M. Nisoli, *Science* **346**, 336 (2014).
6. F. Kelkensberg, W. Siu, J.F. Pérez-Torres, F. Morales, G. Gademann, A. Rouzée, P. Johnsson, M. Lucchini, F. Calegari, J.L. Sanz-Vicario, F. Martín and M.J.J. Vrakking, *Phys. Rev. Lett.* **107**, 043002 (2011).
7. C. Neidel, J. Klei, C.H. Yang, A. Rouzée, M.J.J. Vrakking, K. Klünder, M. Miranda, C.L. Arnold, T. Fordell, A. L'Huillier, M. Gisselbrecht, P. Johnsson, M.P. Dinh, E. Suraud, P.G. Reinhard, V. Despré, M.A.L. Marques and F. Lépine, *Phys. Rev. Lett.* **111**, 033001 (2013).
8. S.R. Leone, C.W. McCurdy, J. Burgdorfer, L.S. Cederbaum, Z. Chang, N. Dudovich, J. Feist, C.H. Greene, M. Ivanov, R. Kienberger, U. Keller, M.F. Kling, Z.-H. Loh, T. Pfeifer, A.N. Pfeiffer, R. Santra, K. Schafer, A. Stolow, U. Thumm and M.J.J. Vrakking, *Nature Photon.* **8**, 162 (2014).
9. D. Kosloff and R. Kosloff, *J. Comp. Phys.* **52**, 35 (1983).
10. K.-J. Yuan and A.D. Bandrauk, *Phys. Rev. A* **84**, 023410 (2011).
11. H. Lu and A.D. Bandrauk, *J. Chem. Phys.* **115**, 1670 (2001).
12. A. Nikodem, R.D. Levine and F. Remacle, *J. Phys. Chem. A* **120**, 3343 (2016).
13. C. Lefebvre, H.Z. Lu, S. Chelkowski and A.D. Bandrauk, *Phys. Rev. A* **89**, 023403 (2014).
14. E. Runge and E.K.U. Gross, *Phys. Rev. Lett.* **52**, 997 (1984).
15. A. Castro, E. Räsänen, A. Rubio and E.K.U. Gross, *Europhys. Lett.* **87**, 53001 (2009).
16. A. Castro, H. Appel, M. Oliveira, C.A. Rozzi, X. Andrade, F. Lorenzen, M.A.L. Marques, E.K.U. Gross and A. Rubio, *Phys. Stat. Solidi B* **243**, 2465 (2006).
17. M.J.T. Oliveira, B. Mignolet, T. Kus, T.A. Papadopoulos, F. Remacle and M.J. Verstraete, *J. Chem. Theo. Comp.* **11**, 2221 (2015).
18. J.J. Bajo, G. Granucci and M. Persico, *J. Chem. Phys.* **140**, 044113 (2014).
19. M. Richter, P. Marquetand, J. González-Vázquez, I. Sola and L. González, *J. Chem. Theo. Comp.* **7**, 1253 (2011).
20. B.F.E. Curchod, T.J. Penfold, U. Rothlisberger and I. Tavernelli, *ChemPhysChem* **16**, 2127 (2015).
21. I. Tavernelli, B.F.E. Curchod and U. Rothlisberger, *Phys. Rev. A* **81**, 052508 (2010).
22. R. Mitrić, J. Petersen and V. Bonačić-Koutecký, *Phys. Rev. A* **79**, 053416 (2009).
23. B.F.E. Curchod, T.J. Penfold, U. Rothlisberger and I. Tavernelli, *Phys. Rev. A* **84**, 042507 (2011).
24. J.C. Tully, *J. Chem. Phys.* **93**, 1061 (1990).
25. M. Ben-Nun, J. Quenneville and T.J. Martínez, *J. Phys. Chem. A* **104**, 5161 (2000).
26. T.J. Martinez, M. Ben-Nun and G. Ashkenazi, *J. Chem. Phys.* **104**, 2847 (1996).
27. S. Álvarez-Barcia, J.R. Flores, G. Granucci and M. Persico, *J. Phys. Chem. A* **117**, 67 (2013).
28. M. Ben-Nun and T.J. Martínez, *Adv. Chem. Phys.* **121**, 439 (2002).
29. M. Ben-Nun and T.J. Martınez, *J. Chem. Phys.* **108**, 7244 (1998).
30. T.J. Martinez, M. Ben-Nun and R.D. Levine, *J. Phys. Chem.* **100**, 7884 (1996).
31. B. Mignolet, B.F.E. Curchod and T.J. Martínez, *Ang. Chem.*, submitted (2016).
32. P.R. Schreiner, H.P. Reisenauer, J. Romanski and G. Mloston, *J. Amer. Chem. Soc.* **132**, 7240 (2010).
33. B.G. Levine, J.D. Coe, A.M. Virshup and T.J. Martínez, *Chem. Phys.* **347**, 3 (2008).
34. D.V. Makhov, W.J. Glover, T.J. Martinez and D.V. Shalashilin, *J. Chem. Phys.* **141**, 054110 (2014).
35. H. Li, B. Mignolet, G. Wachter, J. Burgdörfer, R.D. Levine, F. Remacle and M. Kling, *Phys. Rev. Lett.* **114**, 123004 (2015).
36. M. Kübel, R. Siemering, C. Burger, N.G. Kling, H. Li, A.S. Alnaser, B. Bergues, S. Zherebtsov, A.M. Azzeer and I. Ben-Itzhak, *Phys. Rev. Lett.* **116**, 193001 (2016).
37. C.C. Tannoudji, D. Bernard and L. Franck, (1973).
38. F. Remacle, M. Nest and R.D. Levine, *Phys. Rev. Lett.* **99**, 183902 (2007).
39. J. Ajay, J. Šmydke, F. Remacle and R.D. Levine, *J. Phys. Chem. A* **120**, 3335 (2016).
40. M. Nest, F. Remacle and R.D. Levine, *New J. Phys.* **10**, 025019 (2008).
41. MOLPRO, version 2012.1, a package of ab initio programs. H.-J. Werner, P. J. Knowles, G. Knizia, F. R. Manby, M. Schutz, and others, see http://www.molpro.net.
42. B. Mignolet, R.D. Levine and F. Remacle, *Phys. Rev. A* **89**, 021403 (2014).
43. M.I.S. Röhr, J. Petersen, M. Wohlgemuth, V. Bonačić-Koutecký and R. Mitrić, *ChemPhysChem* **14**, 1377 (2013).
44. B. Mignolet, A. Gijsbertsen, M.J.J. Vrakking, R.D. Levine and F. Remacle, *Phys. Chem. Chem. Phys.* **13**, 8331 (2011).
45. F. Remacle and R.D. Levine, *Phys. Rev. A* **83**, 013411 (2011).
46. D.J. Tannor *Introduction to quantum mechanics*. University Science Books: 2007.
47. J.W. Snyder, B.F.E. Curchod and T.J. Martínez, *J. Phys. Chem. Lett.* **7**, 2444 (2016).